Robust FEM-BEM Coupling for LS-DYNA®'s EM module

Lars Kielhorn, Thomas Rüberg, Jürgen Zechner
TAILSIT GmbH
Nikolaiplatz 4, 8020 Graz, Austria
www.tailsit.com

Abstract

The electromagnetic (EM) solver module of LS-DYNA targets coupled mechanical/thermal/electromagnetic problems as they occur, for instance, in the simulation of metal forming, welding, and induction heating. The EM solver incorporates the coupling of Finite Element and Boundary Element Methods. The main advantage of this approach is that the volume discretization of the surrounding air region is avoided. This approach significantly reduces the modelling time and avoids mesh entanglement due to large deformation of the workpiece in metal forming.
However, the current implementation has severe limitations: Due to the algorithm's explicit character, very small time step sizes are required leading to large simulation times. Moreover, the conditional stability of the current approach only allows for vacuum or materials with very small magnetic permeability.
In this work we present an improved version of that EM module. The new EM module is unconditionally stable with respect to the time step size and allows also for the handling of materials with any permeability.
Besides some inevitable theory the presentation will mainly focus on application examples that confirm the strength of the new EM module.

1. Introduction

Today's development cycles of electric machines, magnetic sensors, or transformers are intimately connected with numerical simulation. A cost-effective development and optimization of these devices is hardly viable without virtual prototyping. The fundamentals of electromagnetic simulations are the Maxwell's equations and one of the most popular and most versatile numerical discretization schemes is the Finite Element Method (FEM). While originally applied to problems in structural mechanics the FEM succeeded also for electromagnetic problems for more than 30 years.

However, the simplicity of the FEM does not come for free. Since electric and magnetic fields extend into the unbounded exterior air region one typically introduces homogeneous boundary conditions some distance away from the solid parts. Then by expanding the Finite Element grid to parts of the air region an approximation for the unknown fields can be obtained. Thanks to the decay properties of the electromagnetic fields this approach is widely applied, accepted, and justified for many applications. Nevertheless, some problems remain:

- Non-physical boundary conditions are imposed on the domain's (fictitious) boundary and the introduced modeling error leads to contaminated solutions. This might become critical when highly accurate simulation results are needed.
- The meshing of the air region requires a considerable amount of time and effort. In many situations the number of elements in the air region even exceeds the number of elements used for the solid parts.
- Electrical devices often contain moving parts. For instance, the variation of the rotor/stator positions of an electric motor requires either a re-meshing of the air gap or a fundamental modification of the Finite Element scheme.
- The accurate computation of electro-mechanical forces with a FEM-only discretization remains a challenge.

A properly designed and implemented FEM-BEM coupling scheme circumvents all of these issues: The Boundary Element Method handles the exterior air region while the solid parts are discretized by the Finite Element Method.

TAILSIT has a strong expertise in the development of numerical simulation tools in general and in Boundary Element Methods in particular. We have implemented a FEM-BEM coupling scheme for electromagnetics [1] that is largely based on theoretical work by R. Hiptmair [2]. Our FEM-BEM solver addresses very similar problems as the FEM-BEM EM module that is shipped with LS-DYNA. However, as it has turned out, LS-DYNA's solver features some weaknesses. E.g., due to an iterative coupling scheme very small time step sizes are required resulting in unnecessary long computation times. In this work we present a remedy for this issue and present a monolithic coupling scheme that is unconditionally stable w.r.t. the time step size. In addition, the monolithic approach allows also for permeable materials. TAILSIT has implemented the monolithic coupling into LS-DYNA and – by March 2018 – proceeds with testing the new solver module.

This work is organized as follows: In Sec. 2 we first recall some general ideas on how different FEM-BEM coupling schemes can be established. In particular, we comment on the differences between indirect and direct methods. LS-DYNA's solver module is based on an indirect coupling while TAILSIT's in-house solver utilizes a direct, symmetric scheme. In Sec. 3 we comment on two solution strategies for the linear block systems that are obtained after Galerkin discretizations of the corresponding variational formulations. We will show that monolithic coupling approaches combined with advanced preconditioning techniques are superior to weak coupling schemes since the latter schemes lack of stability. The numerical examples given in Sec. 4 will confirm the strength of the monolithic coupling as they present simulation results that can be hardly obtained with the current implementation.

2. A short overview on various FEM-BEM coupling schemes

The starting point of the derivation of FEM-BEM coupling schemes for eddy-current problems is the governing equation

$$\mathbf{curl}\,\mu^{-1}\,\mathbf{curl}\,\mathbf{A} + \sigma\partial_t\mathbf{A} = \mathbf{j}_s \qquad \text{in } \Omega^- \subset \mathbb{R}^3 \tag{1}$$

in which $\mathbf{j}_s$ denotes a prescribed current density and $\mathbf{A}$ is the vector potential such that $\mathbf{curl}\,\mathbf{A} = \mathbf{B}$ where $\mathbf{B}$ denotes the magnetic flux density. The parameters μ and $\sigma \geq 0$ are the (possibly nonlinear) magnetic permeability and the electrical conductivity, respectively. The derivative w.r.t. time is denoted by ∂_t. The governing equation holds for all solid parts. They define the *interior* region Ω^-. Contrary, in the complementary exterior air region Ω^+ the vector potential fulfills the linear, homogeneous curl-curl equation

$$\mathbf{curl}\,\mu_0^{-1}\,\mathbf{curl}\,\mathbf{A} = 0 \qquad \text{in } \Omega^+ \tag{2}$$

with μ_0 denoting the vacuum permeability. The variational form of Eqn (1) then reads:
Find $\mathbf{A} \in H(\mathbf{curl}, \Omega^-)$ such that
$$\langle \mu^{-1}\,\mathbf{curl}\,\mathbf{A}, \mathbf{curl}\,\mathbf{A}'\rangle_{\Omega^-} + \langle \sigma\partial_t\mathbf{A}, \mathbf{A}'\rangle_{\Omega^-} - \langle \mu^{-1}\gamma_N^-\mathbf{A}, \gamma_D^-\mathbf{A}'\rangle_\Gamma = \langle \mathbf{j}_s, \mathbf{A}'\rangle_{\Omega^-} \tag{3}$$
for all test functions $\mathbf{A}' \in H(\mathbf{curl}, \Omega^-)$.
The above equation needs some explanation. First, we adopt the notation $\int_M \mathbf{u} \cdot \mathbf{v}\mathrm{d}M = \langle \mathbf{u}, \mathbf{v}\rangle_M$. Further, the space $H(\mathbf{curl}, \Omega^-)$ denotes all vector functions whose $\mathbf{curl}$ is square integrable in Ω^-. The Neumann and Dirichlet trace operators γ_N and γ_D map domain quantities to the boundary $\Gamma = \partial\Omega^-$. Their definitions are

$$\gamma_D^\pm\mathbf{A} = \lim_{\Omega^\pm \ni \tilde{\mathbf{x}} \to \mathbf{x} \in \Gamma} \mathbf{n}(\mathbf{x}) \times \mathbf{A}(\tilde{\mathbf{x}}) \times \mathbf{n}(\mathbf{x})$$
$$\gamma_N^\pm\mathbf{A} = \lim_{\Omega^\pm \ni \tilde{\mathbf{x}} \to \mathbf{x} \in \Gamma} \mathbf{curl}\,\mathbf{A}(\tilde{\mathbf{x}}) \times \mathbf{n}(\mathbf{x}) \tag{4}$$

and the superscript $\pm$ denotes that the trace operation is performed either w.r.t. the interior or exterior domain. In pure Finite Element Methods for electromagnetic problems the traces in Eqn (3) are commonly neglected which is equivalent to either homogeneous Neumann or Dirichlet boundary conditions. This implies that the FEM region must cover also a considerable amount of the unbounded air region such that the assumption of homogeneous boundary conditions is justified due to the decay behavior of the magnetic fields. However, in the context of Boundary Element Methods the trace operators play a crucial role as they allow for a representation via boundary integral operators. The main idea of any FEM-BEM coupling is the following: First, exchange the interior traces in Eqn (3) by their exterior counterparts via suitable transmission conditions. Then, express the exterior traces by boundary integral operators that are related to Eqn (2). The transmission conditions for the eddy-current problem are

$$\gamma_D^- \mathbf{A} = \gamma_D^+ \mathbf{A}$$
$$\mu^{-1}\gamma_N^- \mathbf{A} = \mu_0^{-1}\gamma_N^+ \mathbf{A} \, . \tag{5}$$

Hence, Eqn (5) allows for exchanging the interior Neumann traces by the exterior Neumann traces in the variational form. For simplicity, we skip the superscripts from now on and postulate that all traces are meant to be exterior ones.

Before we give expressions for the BEM operators we need to define the fundamental solution

$$U(\mathbf{z}) = \frac{1}{4\pi} \frac{1}{|\mathbf{z}|} \tag{6}$$

which solves $-\Delta U = 0$ for all $\mathbf{z} \neq 0$. With this we define the Maxwell single and Maxwell double layer potentials

$$(\boldsymbol{\psi}_A \mathbf{u})(\tilde{\mathbf{x}}) = \int_\Gamma U(\tilde{\mathbf{x}} - \mathbf{y})\mathbf{u}(\mathbf{y})\mathrm{d}s_\mathbf{y}$$
$$(\boldsymbol{\psi}_M \mathbf{w})(\tilde{\mathbf{x}}) = \mathbf{curl}_{\tilde{\mathbf{x}}} \int_\Gamma U(\tilde{\mathbf{x}} - \mathbf{y})(\mathbf{w}(\mathbf{y}) \times \mathbf{n}(\mathbf{y}))\mathrm{d}s_\mathbf{y} \, , \qquad \forall \tilde{\mathbf{x}} \in \Omega^+ \, , \mathbf{y} \in \Gamma \, . \tag{7}$$

Above, $\mathbf{n}$ denotes the outward normal vector. Applying the trace operators to the potentials yields the following four boundary integral operators:

$$\mathbf{V}\mathbf{u} = \gamma_D \boldsymbol{\psi}_A \mathbf{u} \qquad \qquad \mathbf{C}\mathbf{w} = \gamma_D \boldsymbol{\psi}_M \mathbf{w}$$
$$\mathbf{C}^* \mathbf{u} = \gamma_N \boldsymbol{\psi}_A \mathbf{u} \qquad \qquad \mathbf{W}\mathbf{w} = -\gamma_N \boldsymbol{\psi}_M \mathbf{w} \, . \tag{8}$$

$\mathbf{V}$ is the *single layer operator*, $\mathbf{C}$ is the *double layer operator*, $\mathbf{C}^*$ is the *adjoint double layer operator*, and $\mathbf{W}$ is the *hypersingular integral operator*.

A non-symmetric, indirect coupling is now achieved by utilizing the ansatz

$$\mathbf{A} = \mu_0 \boldsymbol{\psi}_A \mathbf{k} \tag{9}$$

with some unknown density function $\mathbf{k}$. It can be shown that the ansatz in (9) is a solution of Eqn (2) if the density function has vanishing surface divergence. We denote the space of functions with zero surface divergence by $H(\mathrm{div}_\Gamma\, 0, \Gamma)$.

Now, it remains to put the pieces together: Applying the Dirichlet trace to Eqn (9) and weighting with a test function $\mathbf{k}' \in H(\mathrm{div}_\Gamma\, 0, \Gamma)$ gives a variational formulation for the surface quantities $\gamma_D \mathbf{A}, \mathbf{k}$. Further, we apply the Neumann trace to Eqn (9) and inserting the result $\mu_0^{-1}\gamma_N \mathbf{A} = \mathbf{C}^* \mathbf{k}$ into Eqn (3). This gives the final variational form: *Find* $\mathbf{A} \in H(\mathbf{curl}, \Omega^-)$, $\mathbf{k} \in H(\mathrm{div}_\Gamma\, 0, \Gamma)$ *such that*

$$q(\mathbf{A}, \mathbf{A}') - \langle \mathbf{C}^*\mathbf{k}, \gamma_D\mathbf{A}'\rangle_\Gamma = \langle \mathbf{j}_s, \mathbf{A}'\rangle_{\Omega-}$$
$$\langle \gamma_D\mathbf{A}, \mathbf{k}'\rangle_\Gamma - \mu_0\langle \mathbf{V}\mathbf{k}, \mathbf{k}'\rangle_\Gamma = 0 \tag{10}$$

for all $\mathbf{A}' \in H(\mathbf{curl}, \Omega^-)$, $\mathbf{k}' \in H(\mathrm{div}_\Gamma 0, \Gamma)$.
In Eqn (10), $q(\mathbf{A}, \mathbf{A}')$ abbreviates the bilinear form for the volume terms, i.e.,

$$q(\mathbf{A}, \mathbf{A}') = \langle \mu^{-1}\,\mathbf{curl}\,\mathbf{A}, \mathbf{curl}\,\mathbf{A}'\rangle_{\Omega-} + \langle \sigma\partial_t\mathbf{A}, \mathbf{A}'\rangle_{\Omega-}\;. \tag{11}$$

LS-DYNA's FEM-BEM coupling scheme is based on a proper discretization of Eqn (10). Since the occurring density function $\mathbf{k}$ has no immediate physical meaning this kind of coupling is denoted as indirect, non-symmetric FEM-BEM coupling. A direct, symmetric coupling is achieved if an ansatz via the so-called representation formula is used

$$\mathbf{A} = \boldsymbol{\psi}_A\gamma_N\mathbf{A} + \boldsymbol{\psi}_M\gamma_D\mathbf{A}\;. \tag{12}$$

The equation above expresses the vector potential $\mathbf{A}$ by means of its own traces. Therefore, this approach is entitled as direct method. The formula can be interpreted as the static equivalent to the Stratton-Chu formula [4]. For simplicity, we have deliberately neglected an additional term that deals with the normal trace $\gamma_{\mathbf{n}\mathbf{A}=\mathbf{A}\cdot\mathbf{n}}$ of the vector potential. However, this additional term provides no additional information and is forced to drop out. This is done by imposing the divergence-free constraint to the unknown Neumann trace of $\mathbf{A}$. With the ansatz from Eqn (12), the deduction of the direct coupling follows the same steps as before: Applying the Dirichlet trace to the representation formula gives a boundary integral equation for the unknown Cauchy data $\gamma_D\mathbf{A}, \gamma_N\mathbf{A}$ while the Neumann trace of Eqn (12) is directly incorporated into the variational form from Eqn (3). With the abbreviation $\boldsymbol{\lambda} = \mu_0^{-1}\gamma_N\mathbf{A}$ the final variational form is: *Find* $\mathbf{A} \in H(\mathbf{curl}, \Omega^-)$, $\boldsymbol{\lambda} \in H(\mathrm{div}_\Gamma 0, \Gamma)$ *such that*

$$q(\mathbf{A}, \mathbf{A}') + \mu_0^{-1}\langle \mathbf{W}\gamma_D\mathbf{A}, \gamma_D\mathbf{A}'\rangle_\Gamma - \langle \mathbf{C}^*\boldsymbol{\lambda}, \gamma_D\mathbf{A}'\rangle_\Gamma = \langle \mathbf{j}_s, \mathbf{A}'\rangle_{\Omega-}$$
$$\langle (\mathbf{Id} - \mathbf{C})\gamma_D\mathbf{A}, \boldsymbol{\lambda}'\rangle_\Gamma - \mu_0\langle \mathbf{V}\boldsymbol{\lambda}, \boldsymbol{\lambda}'\rangle_\Gamma = 0 \tag{13}$$

for all $\mathbf{A}' \in H(\mathbf{curl}, \Omega^-)$, $\boldsymbol{\lambda}' \in H(\mathrm{div}_\Gamma 0, \Gamma)$. The operator $\mathbf{Id}$ denotes the identity operator.
Due to the property

$$\langle \mathbf{C}^*\boldsymbol{\lambda}, \gamma_D\mathbf{A}'\rangle_\Gamma = \langle (\mathbf{Id} - \mathbf{C})\gamma_D\mathbf{A}, \boldsymbol{\lambda}'\rangle_\Gamma \tag{14}$$

we have a skew-symmetric system which can be symmetrized such that this coupling scheme is denoted as direct, symmetric FEM-BEM coupling.
Remark: The divergence-free constraints that are imposed on $\mathbf{k}$ and $\boldsymbol{\lambda}$ can be realized via surface curls of some scalar fields. The definition of the surface curl is $\mathbf{curl}_\Gamma = \mathbf{grad}_\Gamma \times\mathbf{n}$ with $\mathbf{grad}_\Gamma = \mathbf{n} \times \mathbf{grad} \times\mathbf{n}$ being the surface gradient. Then, the ansatz $\boldsymbol{\lambda} = \mathbf{curl}_\Gamma\,\varphi$ fulfills the divergence-free constrained due to $\mathrm{div}_\Gamma\,\mathbf{curl}_\Gamma \equiv 0$. However, this approach is not sufficient if one deals with non-simply connected domains. In this case the ansatz has to be augmented by additional surface stream functions. We do not comment further on this issue since these are merely technical details. See [2], [5] for further details.
The Galerkin discretization of the variational forms (10), (13) is straightforward. Using Nedelec elements [6], [7] for the discretization of the FEM operators and RWG elements [8] together with classical piecewise linear functions (e.g. [9]) for the BEM operators gives the block systems

$$\begin{bmatrix} A_\mu & R^\top\widetilde{C}^\top G \\ G^\top MR & -\mu_0 G^\top VG \end{bmatrix} \cdot \begin{bmatrix} \underline{a} \\ \underline{\phi}_k \end{bmatrix} + \begin{bmatrix} M_\sigma & 0 \\ 0 & 0 \end{bmatrix} \cdot \begin{bmatrix} \underline{\dot{a}} \\ \underline{\dot{\phi}}_k \end{bmatrix} = \begin{bmatrix} \underline{f} \\ \underline{0} \end{bmatrix} \tag{15}$$

for the indirect method and

$$\begin{bmatrix} A_\mu + \mu_0^{-1} R^\top W R & R^\top \widetilde{C}^\top G \\ G^\top \widetilde{C} R & -\mu_0 G^\top V G \end{bmatrix} \cdot \begin{bmatrix} \underline{a} \\ \underline{\phi}_\lambda \end{bmatrix} + \begin{bmatrix} M_\sigma & 0 \\ 0 & 0 \end{bmatrix} \cdot \begin{bmatrix} \underline{\dot{a}} \\ \underline{\dot{\phi}}_\lambda \end{bmatrix} = \begin{bmatrix} \underline{f} \\ \underline{0} \end{bmatrix} . \tag{16}$$

for the direct method, respectively. We will comment on the linear systems above in some detail: First of all, $\underline{\dot{x}}$ denotes the time derivative of the vector $\underline{x}$. Further, the matrices A_μ, and M_σ represent the discretized FEM bilinear forms. The matrices V, W, and C stem from the discretization of the boundary integral operators. V and W represent the discrete single layer and hypersingular operators, respectively. The discrete double layer operator is given by the matrix C and we abbreviate $\widetilde{C} = \frac{1}{2}M - C$ with M representing the jump term across the boundary interfaces. The same matrix M occurs in the lower left block of the indirect system (15). The matrix $R: \underline{a} \to \underline{a}_\Gamma$ filters the boundary coefficients of the vector $\underline{a}$, representing the degrees of freedom of the vector potential $\mathbf{A}$. The matrix G realizes the divergence-free constraints. As mentioned before both surface unknowns $\mathbf{k}$ and $\boldsymbol{\lambda}$, are taken from the space $H(\text{div}_\Gamma 0, \Gamma)$. Because of $\text{div}_\Gamma \, \mathbf{curl}_\Gamma \equiv 0$ these functions can be represented as the surface curls of scalar potentials represented by the vectors $\underline{\phi}_k$ and $\underline{\phi}_\lambda$.

3. Solution strategies

A backward Euler scheme can be used for the time discretization of the systems (15), (16). If higher order schemes are desired, we recommend Rosenbrock-Wanner methods [10] in general, and [11] in particular. These schemes reduce the computational costs compared to Runge-Kutta methods considerably.

However, independent of the time integration scheme one is faced with the solution of a two-by-two block system of the form

$$\begin{bmatrix} A & B \\ C & D \end{bmatrix} \cdot \begin{bmatrix} x \\ y \end{bmatrix} = \begin{bmatrix} f \\ g \end{bmatrix} . \tag{17}$$

Currently, LS-DYNA solves such a system via a Gauss-Seidel iteration scheme (see [12], Ch. 3.6). The corresponding fixed point iteration reads (see [13], Ch. 11.2)

$$\underline{x}_{n+1} = T^{-1}\underline{b} + G\underline{x}_n , \quad T = \begin{bmatrix} A & B \\ & D \end{bmatrix}, \, G = Id - T^{-1}S, \, S = \begin{bmatrix} A & B \\ C & D \end{bmatrix}, \, \underline{b} = \begin{bmatrix} f \\ g \end{bmatrix} . \tag{18}$$

The advantage of using this scheme is due to the fact that separate linear solvers for the FEM and BEM system are used. This becomes obvious from the inverse for T

$$T^{-1} = \begin{bmatrix} A^{-1} & \\ & D^{-1} \end{bmatrix} \cdot \begin{bmatrix} Id & -BD^{-1} \\ 0 & Id \end{bmatrix} . \tag{19}$$

Unfortunately, the convergence of this method depends solely on the iteration matrix G. Let $\underline{e}_n$ denote the error in the n-th iteration. We then have

$$\|\underline{e}_n\| \leq \|G\|^n \|\underline{e}_0\| . \tag{20}$$

We refer to [13] for a proof of the above statement. From Eqn (20) it follows that convergence is only guaranteed if the spectral radius of the iteration matrix is less or equal one. Within LS-DYNA, this condition is achieved by imposing a CFL-like condition (see [12], Ch. 3.6)

$$\frac{\sigma \mu_0 h^2}{2\Delta t} \geq 1 \tag{21}$$

with h being the grid's mesh size. As a consequence, the iterative scheme (18) requires very small time step sizes and therefore renders the overall scheme computationally inefficient.

To overcome the restriction posed by Eqn (21) we propose a monolithic coupling for systems like (17). Due to the sheer dimension of the BEM matrices direct solvers are excluded a priori. Contrary, the rate of convergence of iterative solvers based on Krylov subspace methods depends on the conditioning of the system matrix. Therefore, the use of suitable preconditioners is often inevitable. Here, we use a block preconditioner of the form

$$P^{-1} = \begin{bmatrix} P_{\mathrm{FEM}}^{-1} & \\ & P_{\mathrm{BEM}}^{-1} \end{bmatrix} . \tag{22}$$

LS-DYNA always guarantees $\sigma > 0$ such that the FEM preconditioner P_{FEM}^{-1} is based on a LU factorization of the FEM matrix. The preconditioner P_{BEM}^{-1} for the BEM block is simply based on diagonal preconditioning. This preconditioning strategy has been implemented in LS-DYNA and is currently (as of March, 2018) been tested. However, the direct approach for the FEM preconditioner restricts the solver to rather medium sized problems and the diagonal preconditioning for the BEM block is not optimal either. Further, for zero-conductivity regions a factorization of the FEM matrix becomes impossible due to the large kernel of the curl-curl operator. As an alternative we propose a FEM preconditioner that is based on algebraic multigrid methods in conjunction with auxiliary space methods [14]. In addition, an efficient preconditioner for the BEM system is constructed using operator preconditioning techniques [15]. For a deeper analysis of optimal preconditioners we refer to [2]. Here, it suffices to note that the numerical examples provided in the upcoming section are done with TAILSIT's in-house solver which is based on the two last named preconditioning strategies.

Once the block preconditioner is established we use a GMRES solver [16] for the indirect, non-symmetric system and a MINRES solver [17] for the direct, symmetric coupling.

4. Numerical examples

First, we verify the two proposed FEM-BEM coupling schemes by means of an academic example. For this we consider the purely magnetostatic problem of a uniformly magnetized sphere of radius $R = 1$. The constant magnetization is given by $\mathbf{M} = M_0 \mathbf{e}_z$, $M_0 = 1\mathrm{Am}^{-1}$. An analytical solution for this problem can be found in Ch. 5.10 of [18]. We define the relative error as

$$\mathcal{E}(\mathbf{B}_h) = \frac{\|\mathbf{B} - \mathbf{B}_h\|_2}{\|\mathbf{B}\|_2} \tag{23}$$

where $\mathbf{B}$ denotes the analytic magnetic flux density and $\mathbf{B}_h$ is the magnetic flux density computed by the FEM-BEM coupling scheme.

Level	N(tet)	N(tria)	h(tet)	h(tria)
1	32	32	7.22E-01	6.18E-01
2	368	212	4.69E-01	3.16E-01
3	2,035	710	3.57E-01	1.92E-01
4	11,295	2,318	1.86E-01	9.50E-02
5	76,891	9,006	9.50E-02	5.20E-02
6	534,390	35,158	5.80E-02	2.70E-02

Table 1: Volume and surface grid specifications.

The FEM grid consists of curved tetrahedral elements. The grid specifications are given in Tab 1.
The Fig 1 plots the relative errors for various relative permeabilities μ_r against the mesh size of the FEM grid. Obviously, the method works and the convergence behavior is independent of the magnetic permeability.
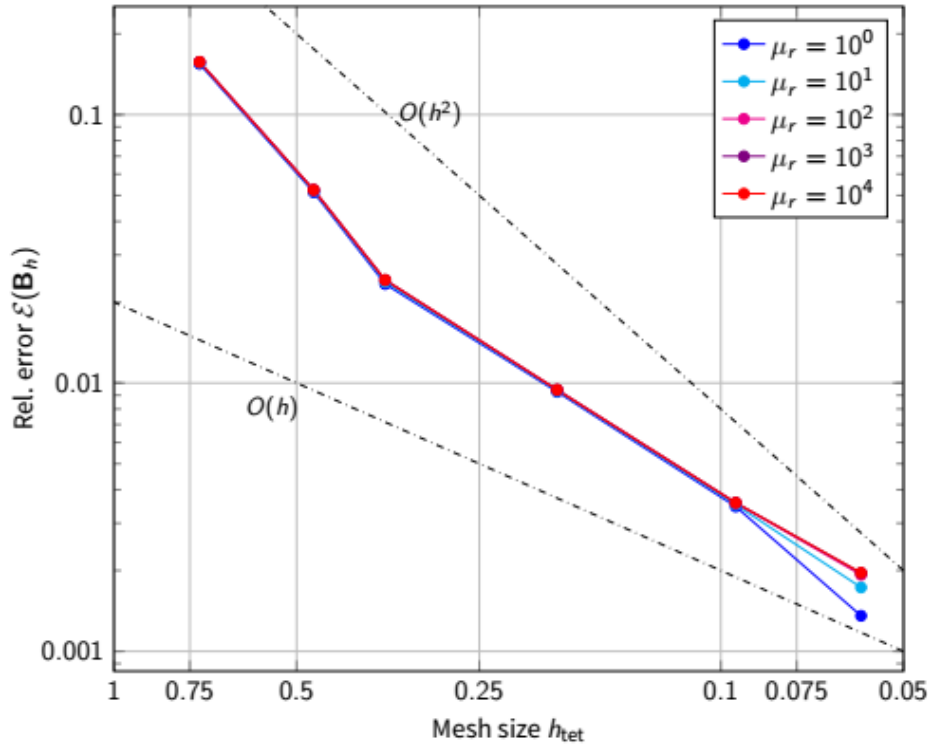
Figure 1: Convergence study. Uniformly magnetized sphere. Direct coupling. MINRES rel. tol. 1E-5

Next, we investigate the efficiency of the preconditioning by means of the iterations that are needed to reduce the residual by five orders of magnitude. The Tab 2 & 3 depict the iteration numbers $It(\mu_r)$ for various relative permeabilities $\mu_r = 10^0, \ldots, 10^4$. While Tab 2 shows the iteration numbers for the direct, symmetric FEM-BEM coupling, the Tab 3 depicts the results that are obtained with the indirect scheme in combination with the diagonal preconditioning of the BEM blocks. The increasing iteration numbers for the indirect scheme are mainly due to the non-optimal BEM preconditioning strategy. Keeping the iteration numbers as low as possible is an important goal – especially since the Boundary Element operators are tackled by a multilevel fast multipole method [19] which realizes a fast matrix-vector multiplication. However, this multiplication is still slower than a matrix-vector product with truly sparse matrices.

Level	It(1)	It(10)	It(100)	It(1000)	It(10000)
2	9	16	21	22	22
3	10	18	24	24	24
4	11	19	25	25	25
5	12	24	29	30	30
6	16	29	35	36	36

Table 2: Direct, symmetric coupling. AMG/AMS FEM preconditioner. BEM preconditioner based on operator preconditioning. Iteration numbers for various permeabilities.

Level	It(1)	It(10)	It(100)	It(1000)	It(10000)
2	17	25	49	81	96
3	22	29	45	57	87
4	30	42	53	66	55
5	49	55	73	82	81
6	66	70	94	101	99

Table 3: Indirect, non-symmetric coupling. AMG/AMS FEM preconditioner. BEM preconditioner based on diagonal scaling. Iteration numbers for various permeabilities.

The next example depicts the results for an *Asymmetrical conductor with a Hole (TEAM7, http://www.compumag.org/jsite/team.html).* Without going into details, the presented FEM-BEM coupling can be formulated also in frequency domain. Fig. 2 shows a contour plot of the real part of the magnetic flux density together with the coil's excitation current and the induced eddy-currents in the plate at a prescribed frequency of 200Hz. Moreover, Fig 3 compares the computed eddy-currents against the measured eddy-currents along a predefined line. Clearly, the computed results are in good accordance with the measurement data.

The final example deals with a classical physical experiment that illustrates the effect of Lenz's law. We consider a magnet falling through a copper pipe. Once the magnet falls through the pipe the direction of the current induced by the changing magnetic field is such that it creates a magnetic field which opposes the change that produced it. The model's parameter are stated in [20]. The FEM-BEM coupling's time integration scheme is based on a Rosenbrock-Wanner method. The time step size is $\Delta t = 0.005s$. As for the TEAM7 example, the simulation is in congruence with the measurement data. In Fig. 4 three snapshots are given that show the falling magnet at times 0.06s, 0.125s, and 0.85s, respectively (additionally, an animated gif is available at http://tailsit.com/lenz/lenz.gif). In this example the benefits of the FEM-BEM coupling really pay off since we deal with a model that consists of moving parts. Moreover, a simulation purely taken out with a Finite Element Method is very involved due to the crucial demand for sophisticated re-meshing facilities.

Acknowledgment
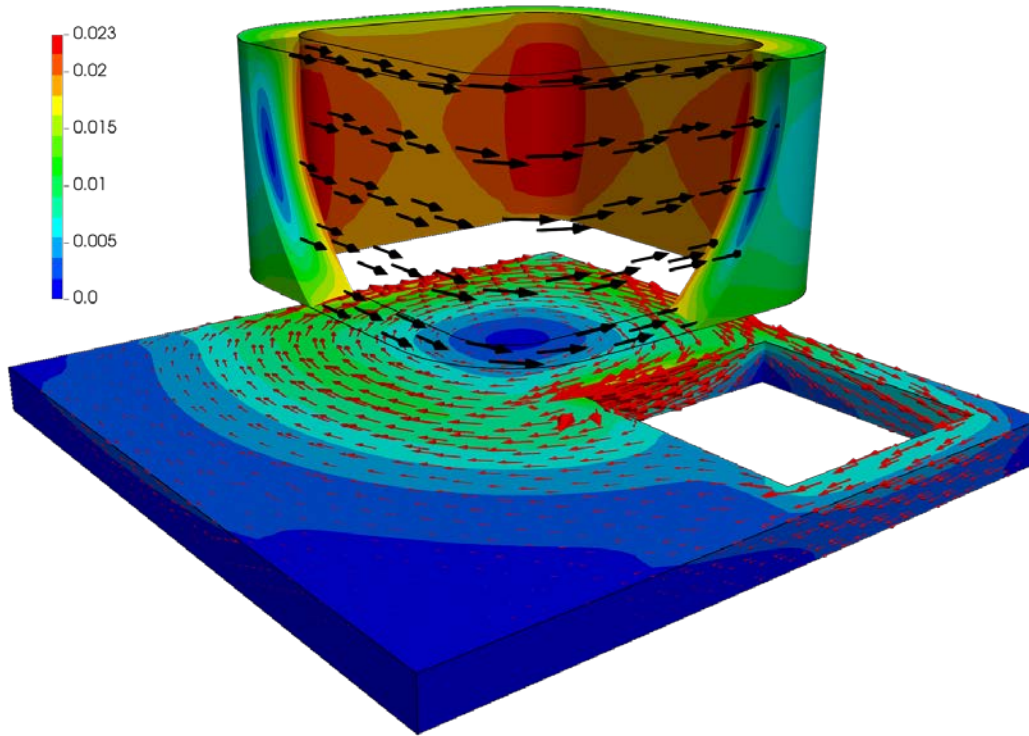
Figure 2: Magnitude of Re(B) with applied current (black) and induced current (red) for 200Hz
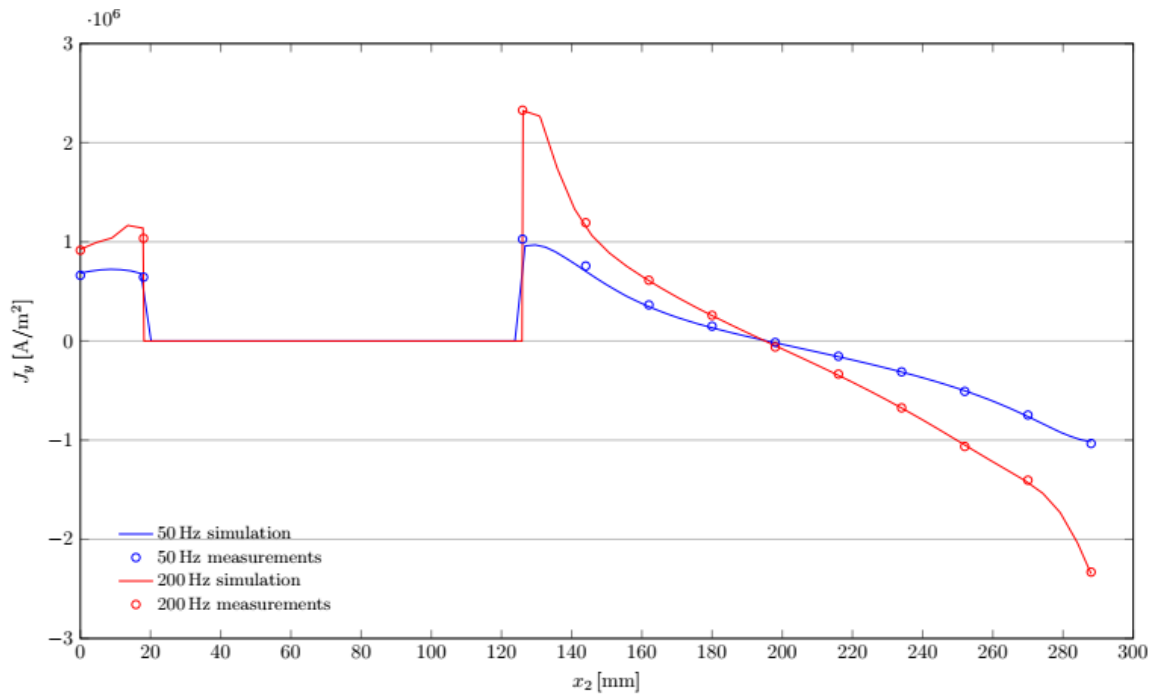
Figure 3: Comparison of induced currents for the frequencies 50Hz and 200Hz along the line 0<x<288mm, y=72mm, z=19mm
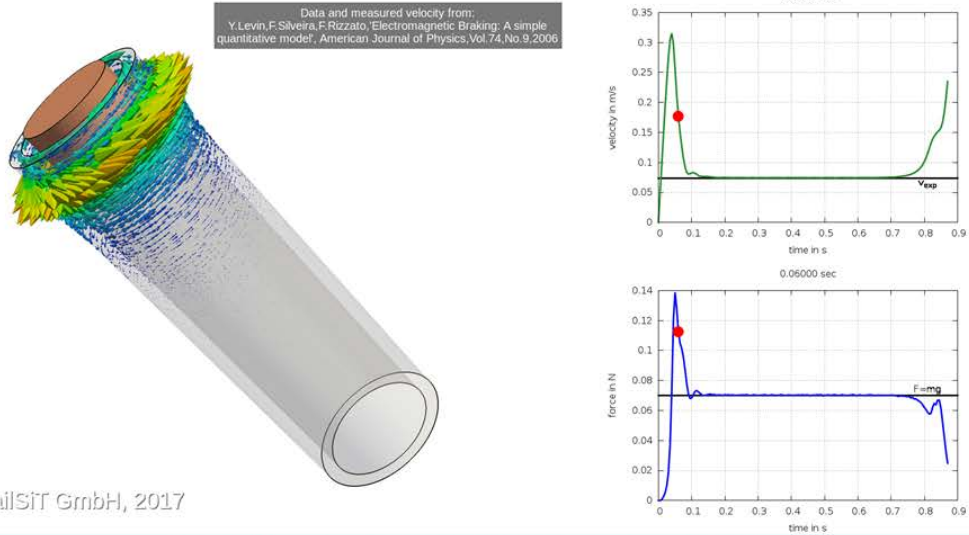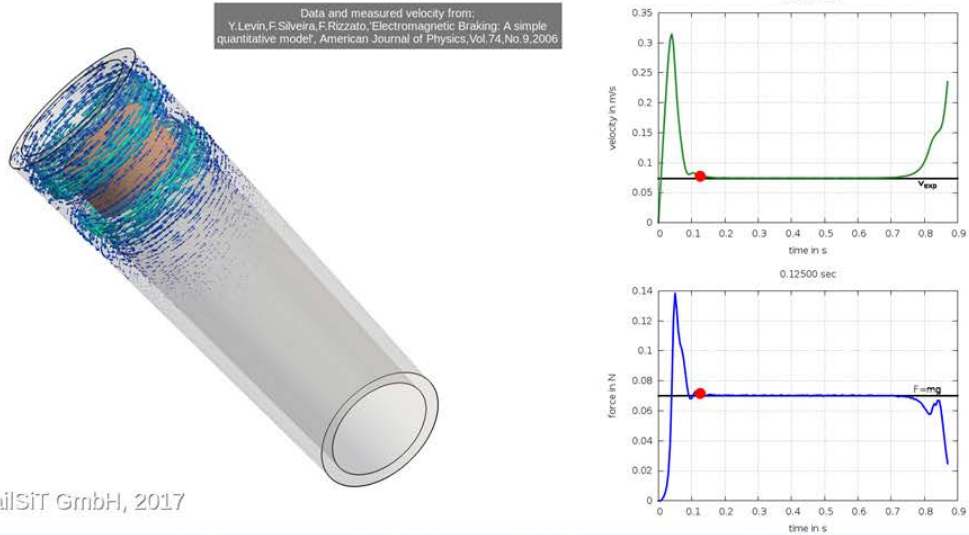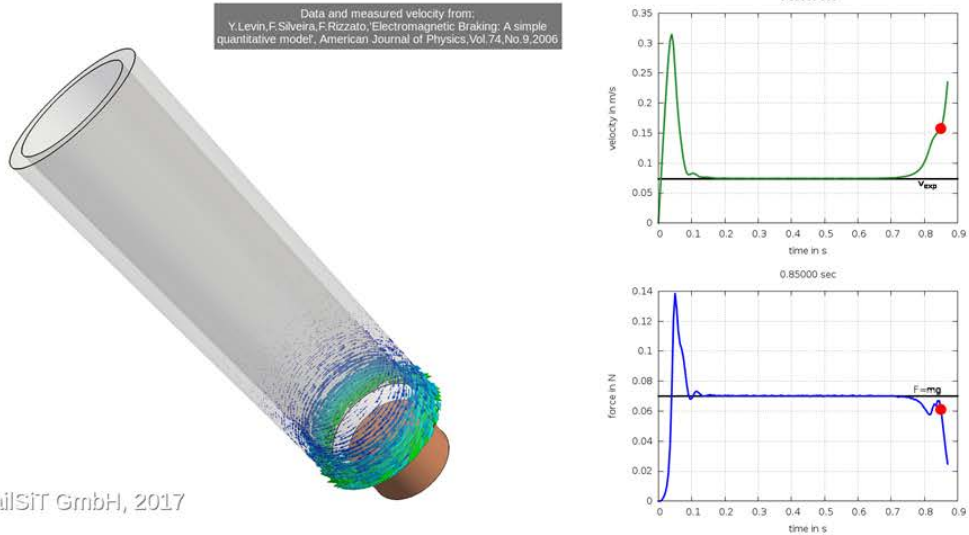
Figure 4: Magnet falling through a copper pipe.

References

[1] L. Kielhorn, T. Rüberg, and J. Zechner, "Simulation of electrical machines: a FEM-BEM coupling scheme," *COMPEL - Int. J. Comput. Math. Electr. Electron. Eng.*, vol. 36, no. 5, pp. 1540–1551, Sep. 2017.

[2] R. Hiptmair, "Symmetric Coupling for Eddy Current Problems," *SIAM J. Numer. Anal.*, vol. 40, no. 1, pp. 41–65, Jan. 2002.

[3] G. C. Hsiao and W. L. Wendland, *Boundary Integral Equations*, vol. 164. Berlin, Heidelberg: Springer Berlin Heidelberg, 2008.

[4] J. A. Stratton and L. J. Chu, "Diffraction Theory of Electromagnetic Waves," *Phys. Rev.*, vol. 56, no. 1, pp. 99–107, Jul. 1939.

[5] R. Hiptmair and J. Ostrowski, "Generators of $H_1(\Gamma_{h},\mathbb{Z})$ for Triangulated Surfaces: Construction and Classification," *SIAM J. Comput.*, vol. 31, no. 5, pp. 1405–1423, Jan. 2002.

[6] J. C. Nedelec, "Mixed finite elements in R3," *Numer. Math.*, vol. 35, no. 3, pp. 315–341, Sep. 1980.

[7] M. Bergot and M. Duruflé, "High-order optimal edge elements for pyramids, prisms and hexahedra," *J. Comput. Phys.*, vol. 232, no. 1, pp. 189–213, Jan. 2013.

[8] S. Rao, D. Wilton, and A. Glisson, "Electromagnetic scattering by surfaces of arbitrary shape," *IEEE Trans. Antennas Propag.*, vol. 30, no. 3, pp. 409–418, May 1982.

[9] A. Ern and J.-L. Guermond, *Theory and Practice of Finite Elements*, vol. 159. New York, NY: Springer New York, 2004.

[10] E. Hairer and G. Wanner, *Solving Ordinary Differential Equations II*, vol. 14. Berlin, Heidelberg: Springer Berlin Heidelberg, 1996.

[11] D. Lanser, J. G. Blom, and J. G. Verwer, "Time Integration of the Shallow Water Equations in Spherical Geometry," *J. Comput. Phys.*, vol. 171, no. 1, pp. 373–393, Jul. 2001.

[12] "EM THEORY MANUAL - Electromagnetism and Linear Algebra in LS-DYNA." Aug-2012.

[13] G. H. Golub and C. F. Van Loan, *Matrix computations*, vol. 3. JHU Press, 2012.

[14] R. Hiptmair and J. Xu, "Nodal Auxiliary Space Preconditioning in H(curl) and H(div) Spaces," *SIAM J. Numer. Anal.*, vol. 45, no. 6, pp. 2483–2509, Jan. 2007.

[15] O. Steinbach and W. L. Wendland, "The construction of some efficient preconditioners in the boundary element method," *Adv. Comput. Math.*, vol. 9, no. 1/2, pp. 191–216, 1998.

[16] Y. Saad and M. H. Schultz, "GMRES: A Generalized Minimal Residual Algorithm for Solving Nonsymmetric Linear Systems," *SIAM J. Sci. Stat. Comput.*, vol. 7, no. 3, pp. 856–869, Jul. 1986.

[17] C. C. Paige and M. A. Saunders, "Solution of Sparse Indefinite Systems of Linear Equations," *SIAM J. Numer. Anal.*, vol. 12, no. 4, pp. 617–629, Sep. 1975.

[18] J. D. Jackson, *Classical Electrodynamics*, 3rd ed. John Wiley & Sons, Inc., 1999.

[19] L. Greengard and V. Rokhlin, "A new version of the Fast Multipole Method for the Laplace equation in three dimensions," *Acta Numer.*, vol. 6, p. 229, Jan. 1997.

[20] Y. Levin, F. L. da Silveira, and F. B. Rizzato, "Electromagnetic braking: a simple quantitative model," Mar. 2006.